Single-particle properties of a model for coexisting charge and spin quasi-critical fluctuations coupled to electrons

S. Caprara, M. Sulpizi, A. Bianconi, C. Di Castro, and M. Grilli

Dipartimento di Fisica - Università di Roma "La Sapienza"

and Istituto Nazionale di Fisica della Materia, Unità di Roma 1

P.le A. Moro, 2 - 00185 Roma - Italy

Abstract

We study the single-particle spectral properties of a model for coexisting AFM and ICDW critical fluctuations coupled to electrons, which naturally arises in the context of the stripe-quantum-critical-point scenario for high-T_c superconducting materials. Within a perturbative approach, we show that the on-shell inverse scattering time deviates from the normal Fermi-liquid behavior near the points of the Fermi surface connected by the characteristic wave-vectors of the critical fluctuations (hot spots). The anomalous behavior is stronger when the hot spots are located near singular points of the electronic spectrum.

The violations to the normal Fermi-liquid behavior are associated with the transfer of spectral weight from the quasi-particle peak to incoherent shadow peaks, which produces an enhancement of incoherent spectral weight near the Fermi level.

We use our results to discuss recent ARPES experiments on Bi2212 near optimal doping.

PACS: 71.10.Hf, 71.45.Lr, 74.25.Jb

I. INTRODUCTION

The nature of the single-particle excitations in a metal close to a Quantum Critical Point (QCP) has become a subject of interest after the proposal that the anomalous properties of the metallic phase of high-T_c superconductors may be related to the presence of a singular effective scattering amplitude, such as the one arising near a QCP of some kind of instability, in the Random Phase Approximation (RPA). Two realization of this scenario have been proposed, the first associated with an antiferromagnetic (AFM) instability [1–3], the second with an incommensurate charge-density-wave (ICDW) instability [4].

The presence of an AFM phase at zero and very low doping and of strong AFM fluctuations, revealed in neutron-scattering experiments at higher doping [5], has suggested that the relevant physics of high-T_c superconducting materials is dominated by the AFM QCP. However in such scenario the QCP itself is quite far from the point of optimal doping where both the highest T_c and the maximum violations of the Fermi-liquid (FL) behavior in the metallic phase are observed. To explain this evident inconsistency strong vertex corrections have to be advocated in order to suppress the effect of AFM fluctuations [6], which would otherwise be strongest at lower doping, close to the QCP. Moreover the peculiar role of the optimal-doping point in all classes of high-T_c materials is left unexplained.

To avoid this problem, and considering also that previous theoretical results indicate the presence of a charge instability, the existence of a new QCP was proposed, which controls the physics of the cuprates near optimal doping. Indeed, models for strongly correlated electrons with short-range interactions are commonly characterized by an instability with respect to phase separation [7], which is turned into an instability with respect to ICDW when long-range Coulomb forces are taken into account [4,8].

The most direct evidence for a new QCP at (or near to) optimal doping is provided by resistivity measurements [9], which reveal an insulator-to-metal transition when the superconducting state is suppressed by a strong pulsed magnetic field. Neutron scattering experiments evidenced charge-driven order in related compounds [10]. Coexistence of ICDW and

electron gas has been detected in joint EXAFS [11,12] and X-ray diffraction [13] experiments (see also Ref. [14]).

The new QCP is not incompatible with an AFM QCP. The two coexist and determine the physics of high-T_c superconducting materials in different regions of the phase diagram. Near optimal doping it is very likely that charge degrees of freedom play a major role. Moreover the dynamical charge segregation into hole-rich and hole-poor regions, associated with critical charge fluctuations, would enhance AFM fluctuations far away from the AFM QCP, due to the natural tendency of hole-poor regions towards antiferromagnetism. In this way a consistent framework is achieved to understand the role of spin degrees of freedom in optimally doped and overdoped materials. AFM fluctuations enslaved by the onset of charge dynamical fluctuations were evidenced in related compounds [10].

Different approaches have been used so far to capture the relevant features of the single-particle excitation spectra in a metal close to a QCP. In the mean-field theory of spin-density-wave (SDW) antiferromagnetism the quasi-particle spectrum may be obtained by coupling the electrons to spin fluctuations characterized by a factorized susceptibility $\chi = i\pi S(S+1)\delta(\omega)\delta(q-Q)$, where $Q = (\pi/a, ..., \pi/a)$ is the wave-vector of the AFM structure and S is the spin quantum number of the fluctuating spin. Within this approach the gap in the quasi-particle spectrum is proportional to the effective coupling g. Kampf and Schrieffer proposed that the resulting self-energy $\Sigma(k,\varepsilon) = g^2[(\varepsilon - \xi_{k-Q})^{-1} - i\pi \mathrm{sgn}(\varepsilon)\delta(\varepsilon - \xi_{k-Q})]$, could be slightly modified, near the AFM QCP, due to the interaction between free electrons and AFM fluctuations [15,16], which leads to a broadening $|\mathrm{Im}\Sigma| \simeq g^2\Gamma/[(\varepsilon - \xi_{k-Q})^2 + \Gamma^2]$ so that $\mathrm{Re}\Sigma \simeq g^2(\varepsilon - \xi_{k-Q})/[(\varepsilon - \xi_{k-Q})^2 + \Gamma^2]$ has a quasi-polar structure [17]. Thus the inverse scattering time at the Fermi energy is finite $1/\tau \simeq 2\Gamma/[\xi_{k-Q}^2 + \Gamma^2]$ and new (quasi-)poles appear in the electron Green function at energies $\varepsilon \sim \xi_{k-Q}$, which are usually called shadow bands.

Within the framework of the nearly-AFM FL (NAFL) [2], Chubukov *et al.* [6], investigated the single-particle properties of a model for electrons coupled to spin fluctuations characterized by a phenomenological susceptibility of the form proposed by Millis, Monien

and Pines [18]. An undamped susceptibility $\chi(q,\omega)$ was used to describe mainly the underdoped region. Within perturbation theory a topological transition of the Fermi surface (FS) was found at a finite value of the electron-spin fluctuations coupling constant [6], leading to the formation of hole pockets located around the points $(\pm\pi/2a, \pm\pi/2a)$ of the Brillouin zone. Such a transition is associated with the appearance of new poles in the electron Green function which are the result of the evolution of the electron self-energy towards a mean-field-like behavior similar to that suggested in Ref. [15,16]. Thus, in this scenario, the precursors of the AFM phase show up in the anomalous metallic phase, at higher doping, with a change in the nature of the quasi-particles, signalling the incipient antiferromagnetism.

However the experimental results provide an increasing evidence for the existence of stripe phases with modulations incommensurate with the lattice [19]. This makes at least questionable a description in terms of AFM fluctuations only. Moreover, the topology of the FS of optimally doped Bi2212 was recently determined with great accuracy [20], revealing new relevant features, and namely an asymmetric suppression of the spectral weight near the Fermi level around the M points of the Brillouin zone, at points of the FS connected by an incommensurate wave-vector $Q_c = (0.4\pi/a, -0.4\pi/a)$, in addition to a symmetric suppression at the same points, associated with the wavevector $Q_s = (\pi/a, \pi/a)$.

This may be interpreted within the ICDW QCP scenario [4], as a signature of quasi-critical charge fluctuations close to a stripe phase. In the following we want to check the consistency of this interpretation, and suggest that ARPES experiments can be used to extract the properties of the charge-fluctuation spectrum, from the related features appearing in the single-particle excitation spectra.

Since we expect that the onset of a stripe phase reintroduces AFM fluctuations, we consider as a starting point an effective model for coexisting charge and spin fluctuations coupled to conduction electrons with bare band dispersion ξ_k. The properties of such charge and spin fluctuations are generically described within a RPA around the QCP at optimal doping, which can be considered as the point governing the onset of the stripe phase. The explicit form of the parameters appearing in the resulting charge and spin susceptibilities,

which depend on the underlying microscopic model, will be deduced below by means of a phenomenological analysis, mainly based on ARPES experiments. In particular, the modulation of the density waves associated with charge and spin fluctuations is characterized by the wave-vectors Q_c and Q_s respectively.

Within a perturbative approach we show that such a model exhibits a violation of the normal FL behavior associated with the transfer of spectral weight from the quasi-particle peak at an energy $\varepsilon \simeq \xi_k$ to dispersing incoherent bands located at $\varepsilon \simeq \xi_{k-Q_{c,s}}$, without the appearance of new poles in the electron Green function. The resulting bands have thus the aspect, but not the coherent nature of the shadow bands found within the approaches of Refs. [6,15]. Such bands could be related to corresponding broad features seen in ARPES experiments, such as the peak at an energy $\varepsilon \simeq -200$ meV, observed near the M points of the Brillouin zone in Bi2212 [21].

We point out that the shadow features of incoherent nature were also found by Bennemann *et al.* within the FLEX approximation for the Hubbard model [22]. The interpretation of the shadow bands as spectral-weight anomalies [23] was also suggested in ref. [24]. More recently similar results were found within the NAFL scenario [25], by performing a full re-summation of the entire perturbation series in the high-temperature (static) limit for the spin-fluctuation spectrum. We point out that these results agree with our simpler perturbative results, in the case of electrons coupled to spin fluctuations only. Moreover, by considering also the effect of charge fluctuations, we reproduce new features, which have a counterpart in recent ARPES experiments, and call for further investigation.

The scheme of the paper is the following. In Sec. II we introduce the model for tight-binding electrons coupled to charge and spin fluctuations. In Sec. III we discuss the violation of the FL behavior for the on-shell inverse scattering time. In Sec. IV we analyze the single-particle spectral properties of our model. Sec. V is devoted to the comparison between our results and ARPES experiments on Bi2212 near optimal doping. Concluding remarks are found in Sec. VI.

II. THE MODEL

We consider a model for tight-binding electrons coupled to charge and spin fluctuations, described by the Hamiltonian

$$\mathcal{H} = \sum_{k,\sigma} (\xi_k - \delta\mu)\, c^+_{k,\sigma} c_{k,\sigma} + \sum_i g_i \sum_{kq,\alpha\beta} c^+_{k+q,\alpha} c_{k,\beta} \tau^i_{\alpha\beta} S^i_{-q}, \tag{1}$$

where $\xi_k = -2t[\cos(k_x a) + \cos(k_y a)] - 4t' \cos(k_x a)\cos(k_y a) - \mu$ is the dispersion law for free electrons on a square bi-dimensional lattice for the CuO_2 planes with hopping terms up to next-to-nearest neighbors included, a is the lattice spacing, and μ is the bare chemical potential. In the following, for the sake of definiteness, and aiming in the end for a comparison with ARPES experiments, we assume that $-1 < 2t'/t < 0$, to fix the main properties of the bare band structure and the shape of the FS, as appropriate to the Bi2212 samples. The correction $\delta\mu \sim O(g^2)$ to the chemical potential is treated perturbatively and is fixed to ensure that the number of particles is the same as that in the free-electron system with bare chemical potential μ.

The second term in (1) describes the interaction of electrons with charge ($i = 0$) and spin ($i = 1, 2, 3$) fluctuating fields S^i_{-q}, which is characterized by the coupling constants g_i. The spin structure of the generalized electron density coupled to the fluctuating field S^i_{-q} is given by the corresponding Pauli matrix τ^i. We assume that the phenomenological properties of the fluctuating fields S^i_{-q} are completely described by correlation functions of the form

$$\chi_{ij}(q, \omega) = \frac{\delta_{ij} A_j}{\Omega_j(q) - i\omega}, \tag{2}$$

where, for each j, A_j is some constant, $\Omega_j(q) = M_j + \alpha_j T + \nu_j \gamma_{q-Q_j}$ with $\gamma_q = 2 - \cos(q_x a) - \cos(q_y a)$, Q_j is the characteristic wave-vector of the critical fluctuations, ν_j is the inverse of the characteristic time scale of the fluctuating mode and the distance from criticality is measured by the "mass term" $M_j + \alpha_j T$. In particular M_j is the distance from the QCP at zero temperature, which we assume to depend on the hole doping per unit cell x and to vanish at a critical value x_c, and T is the temperature in energetic units, so that

α_j is a dimensionless constant. We point out that the cos-like form of the dispersion in $\gamma(q)$ is adopted to reproduce a q^2 behavior at small momenta, while preserving the lattice periodicity [4].

We further assume complete spin isotropy, so that all the above parameters are the same for $j = 1, 2, 3$. Thus in the following we turn to the notation $j = c, s$ for all the constants related to charge and spin fluctuating fields respectively. We also introduce the dimensionless coupling constants $\lambda_c = g_c^2 A_c / t\nu_c$ and $\lambda_s = g_s^2 A_s / t\nu_s$.

In the case of AFM fluctuations the susceptibility (2) corresponds to the phenomenological expression obtained by Millis, Monien and Pines [18] in the limit of strong damping; in the case of ICDW a similar expression was found close to the instability in the Hubbard-Holstein model with long-range Coulomb forces, within a slave-boson approach [4,8]. In the present phenomenological approach the fact that charge instability leads to an enslaved spin modulation at the stripe QCP, is modelled by the requirement that the vanishing of the mass M_s is guided by the vanishing of the mass M_c. The determination of explicit dependence of M_s on M_c requires the introduction of a specific microscopic model, which is beyond the scope of this paper. We point out that, in the static limit $\omega \to 0$, and for momenta $q \ll 1/a$, the susceptibilities (2) have the form of the Ornstein-Zernicke critical correlation function.

Close to criticality ($T, M_j \ll t$) a perturbative analysis is in principle not justified. Nonetheless, to capture the essential features of the single-particle spectra when electrons are coupled through a singular effective interaction, we perform our calculations within perturbation theory. The agreement with the full calculations [25] in the static limit, as well as the claimed smallness of vertex corrections [6], provide a support to the substantial validity of our approach. Since a full microscopic derivation of the parameters appearing in our model would not be appropriate in this context, we rather follow a phenomenological analysis, based on the interpretation of experimental results.

The lowest order in perturbation theory gives an electron self-energy

$$\Sigma(k, \varepsilon) = \Sigma_c(k, \varepsilon) + 3\Sigma_s(k, \varepsilon) - \delta\mu, \tag{3}$$

where a factor of 3 in front of Σ_s comes out from the sum over the three spin components $j = 1, 2, 3$, which are equivalent in the paramagnetic phase. We discuss the single-particle spectral properties by means of the spectral density

$$A(k,\varepsilon) = \frac{1}{\pi} \frac{|\mathrm{Im}\Sigma(k,\varepsilon)|}{[\varepsilon - \xi_k - \mathrm{Re}\Sigma(k,\varepsilon)]^2 + [\mathrm{Im}\Sigma(k,\varepsilon)]^2}. \tag{4}$$

The correction $\delta\mu$ to the chemical potential is fixed, for a given set of coupling constants $\{\lambda_j\}$, by the condition

$$2 \int_{-\pi/a}^{\pi/a} \int_{-\pi/a}^{\pi/a} \frac{d^2k}{(2\pi/a)^2} \int_{-\infty}^{+\infty} A(k,\varepsilon) f(\varepsilon) d\varepsilon = 1 - x, \tag{5}$$

where x is the hole doping per unit cell with respect to half filling, and a factor of 2 in the l.h.s. accounts for spin degeneracy. The self-energies appearing in (3) are calculated at a fixed value of the bare chemical potential μ, which corresponds to the same hole doping x. The explicit expression for the imaginary part of the self-energies appearing in (3) is

$$\mathrm{Im}\Sigma_j(k,\varepsilon) = \lambda_j \nu_j t \mathrm{sgn}(\varepsilon) \int_{-\pi/a}^{\pi/a} \int_{-\pi/a}^{\pi/a} \frac{d^2k'}{(2\pi/a)^2} \frac{[\varepsilon - \xi_{k'}][f(\xi_{k'}) + b(\xi_{k'} - \varepsilon)]}{[\varepsilon - \xi_{k'}]^2 + \Omega_j^2(k - k')}, \tag{6}$$

where $f(\varepsilon) = [e^{\varepsilon/T} + 1]^{-1}$ is the Fermi function, and $b(\varepsilon) = [e^{\varepsilon/T} - 1]^{-1}$ is the Bose function. Within our approach the momentum cut-off $q_{max} = \pi/a$ is provided by the underlying lattice. Since, however, we assumed the specific form (2) for the susceptibilities, which is expected to hold for momenta $q \simeq Q_j$, we introduce in (6) a smooth cut-off function $\mathcal{C}_\Delta(k - k' - Q_j) = \exp(-\gamma_{k-k'-Q_j}/\Delta^2)$, whenever a quantitative improvement is needed to compare with experimental results. We point out that the presence of a finite cut-off Δ does not change the qualitative behavior of the quantities under discussion.

At $T = 0$ the integral over k' in (6) is restricted to the region $0 \leq \xi_{k'} \leq \min(\varepsilon, \xi_{max})$ for $\varepsilon > 0$ and $\max(\varepsilon, \xi_{min}) \leq \xi_{k'} \leq 0$ for $\varepsilon < 0$, where $\xi_{min} \equiv -2t - 4t' - \mu$ and $\xi_{max} = 2t - 4t' - \mu$ are the minimum and the maximum over k of ξ_k (in the parameter range $-1 < 2t'/t < 0$).

The real part of each self-energy is obtained as the Kramers-Krönig transformation (KKT) of the corresponding imaginary part (6),

$$\mathrm{Re}\Sigma_j(k,\varepsilon) = \frac{P}{\pi} \int_{-\infty}^{+\infty} \frac{d\omega}{\omega - \varepsilon} \mathrm{Im}\Sigma_j(k,\omega) \mathrm{sgn}(\omega). \tag{7}$$

Equations (6) and (7) are the starting point to obtain single-particle physical properties such as the on-shell inverse scattering time, the spectral density (4) and the characteristic features of the FS which will be discussed in the following sections.

III. ON-SHELL INVERSE SCATTERING TIME.

The inverse scattering time provides an indication of the violation of the normal FL behavior near criticality (i.e. for $M_j, T \ll t$). At the lowest order in perturbation theory the on-shell inverse scattering time for a quasi-particle with energy $\xi_k > 0$ at $T = 0$ is

$$\left(\frac{1}{\tau_k}\right)_j \equiv -2\mathrm{Im}\Sigma_j(k,\xi_k) = 2\lambda_j\nu_j t \int\int_{k':\ 0\le\xi_{k'}\le\xi_k} \frac{d^2k'}{(2\pi/a)^2} \frac{\xi_k - \xi_{k'}}{[\xi_k - \xi_{k'}]^2 + \Omega_j^2(k-k')} \tag{8}$$

for each scattering channel j. In this section, as a matter of illustration, we consider the effect of a single quasi-critical mode, dropping the index j. We discuss the generic behavior of $1/\tau_k$ and individuate the regions where the strongest violations to the FL behavior take place. When more than one quasi-critical mode is considered, the resulting behavior is dominated by the most singular contribution. For a given k the two terms in the denominator of (8) do not vanish simultaneously unless $\xi_k = \xi_{k-Q}$. Then the most important contribution to (8) comes from a region around the point $k' = k - Q$, where $\xi_{k'} = \xi_k$ and $\Omega(k-k') = M$. We take $\Omega(k-k') \simeq M + \nu a^2(|k-Q|^2\phi^2 + \rho^2)/2$ where $\rho \equiv |k'| - |k-Q| \simeq (\xi_{k'} - \xi_{k-Q})/v_{k-Q}$, $|\rho| \ll |k-Q|$, v_{k-Q} is the velocity of electrons at the point $k-Q$, and ϕ is the (small) angle between k' and $k-Q$. The low-energy behavior of $1/\tau_k$ is most singular when k varies along the line $\xi_k = \xi_{k-Q}$, which meets the FS at the "hot-spot" where $k_F \equiv k_{HS}$, such that $\xi_{k_{HS}} = \xi_{k_{HS}-Q} = 0$. Then we take $\Omega(k-k') \simeq M + \nu a^2|k_{HS} - Q|^2\phi^2/2$ and we perform the integral over ρ in (8), finding

$$\frac{1}{\tau_k} \simeq \frac{2\lambda t\nu |k_{HS}-Q| a^2\sqrt{\xi_k}}{v_{k_{HS}-Q}} \int_0^\infty d\theta \log\left[1 + \left(\frac{M}{\xi_k} + \frac{\nu a^2|k_{HS}-Q|^2}{2}\theta^2\right)^{-2}\right], \tag{9}$$

where $\theta = \phi/\sqrt{\xi_k}$ and the upper limit is extended to ∞, to extract the leading behavior. At the QCP $M = 0$ and the integration over θ yields the non-FL behavior [26]

$$\frac{1}{\tau_k} \simeq \frac{\lambda t a \nu}{v_{k_{HS}-Q}} \sqrt{\frac{\xi_k}{\nu}}. \tag{10}$$

When $M > 0$ two different regimes exist. For $\xi_k \gg M$ the behavior (10) is again found, whereas for $\xi_k \ll M$ the mass term prevents the denominator in (8) from vanishing and the FL behavior [26]

$$\frac{1}{\tau} \simeq \frac{\lambda t a \sqrt{\nu M}}{v_{k_{HS}-Q}} \left(\frac{\xi_k}{M}\right)^2 \tag{11}$$

is recovered. When k approaches k_F along a line on which $\xi_k \neq \xi_{k-Q}$, we take $\Omega(k-k') \simeq M^* + \nu a^2 |k_F - Q|^2 \phi^2/2$, where $M^* = M + \nu a^2 \xi^2_{k_F-Q}/v^2_{k_F-Q}$ is, in this case, the energy scale which separates the FL regime from the anomalous regime and is in general finite at the QCP, leading to a FL behavior for $0 < \xi_K \ll M^*$. In this case Eq. (11) holds with $M \to M^*$, $k_{HS} \to k_F$. The maximum violation of the FL behavior is found for $M^* = 0$, i.e. $M = 0$ and $\xi_{k_F-Q} = 0$ (i.e. $k_F = k_{HS}$), in which case Eq. (10) holds down to $\xi_k = 0$.

We study the dimensionless quantity $1/\lambda\nu\tau_k$ as a function of ξ_k/ξ_{max}, according to (8), in the case when k approaches k_{HS} as $\xi_k \to 0$. In this case the asymptotic behavior (10) and (11) are recovered according to the value of the energy scale M (i.e. the distance from the QCP). For the sake of definiteness we fix the parameters of the electronic spectrum as $t'/t = -0.25$, and the parameters of the fluctuation spectrum as $\nu/t = 5.0$, $Q = (\pi/a, \pi/a)$. For this value of the characteristic wave-vector the hot spots within the first Brillouin zone can be determined analytically as the intersections between the FS ($\xi_k = 0$) and the four lines $k_y = \pm\pi/a \pm k_x$. One hot spot is $k_{HS} = (a^{-1}\arccos\sqrt{\mu/4t'}, \pi/a - a^{-1}\arccos\sqrt{\mu/4t'})$, and the others are found by applying all the symmetry transformations $\mathcal{R}$ of the point group. We leave the ratio μ/t (or equivalently the hole doping x) as a parameter to change the position of the Fermi level and the location of the hot spots, and to discuss the resulting different regimes. We also let M/t vary in the range $[10^{-6}; 10^{-1}]$, to explore the cross-over from the non-FL regime to the FL regime for k approaching k_{HS}.

In Fig. 1(a) we take $\mu/t = -0.9$ (corresponding to a hole doping $x = 0.17$), i.e. $k_{HS} = (0.32/a, 2.82/a)$. As M/t is reduced (by a factor of ten for each curve from bottom to top),

the square-root behavior (10) extends over a wider range of energies. In particular, within the energy range considered in Fig. 1(a), the bottom curve ($M/t = 10^{-1}$) displays a FL behavior (11), whereas the top curve ($M/t = 10^{-6}$) displays a non-FL behavior (10). The intermediate curves show the crossover from one regime to the other.

The above analysis has to be refined if the point $k_{HS} - Q$ on the FS is close to a singular point of the electronic spectrum so that $v_{k_{HS}-Q}$ is small. For instance, the characteristic wave-vector $Q_s = (\pi/a, \pi/a)$ of the AFM fluctuations connects the M points $k = (\pi/a, 0)$ and $k' = (0, -\pi/a)$, or equivalently $(0, \pi/a)$, of the Brillouin zone, where saddle-point van Hove singularities exist at an energy $\xi_{VH} = 4t' - \mu$. A more accurate calculation is needed, as the chemical potential approaches $\bar{\mu} \equiv 4t'$ and $v_{k_F-Q} \sim \sqrt{|\mu - \bar{\mu}|}$, making the estimates (10, 11) meaningless. In the limiting case $\mu = \bar{\mu}$, $v_{k_F-Q} = 0$ and we find

$$\frac{1}{\tau_k} \simeq 8\lambda\nu t a^2 \int_0^\infty dy \int_{y\sqrt{m_x/m_y}}^{\sqrt{2m_x + m_x y^2/m_y}} dx \frac{1 - \frac{x^2}{2m_x} + \frac{y^2}{2m_y}}{\left(1 - \frac{x^2}{2m_x} + \frac{y^2}{2m_y}\right)^2 + \left[\frac{M}{\xi_k} + \frac{\nu a^2}{2}(x^2 + y^2)\right]^2}, \qquad (12)$$

where $1/m_x = a^2(2t + 4t')$, $1/m_y = a^2(2t - 4t')$, $x = k'_x/\sqrt{\xi_k}$ and $y = (k'_y - \pi/a)/\sqrt{\xi_k}$. At the QCP $M = 0$ and (12) is independent of ξ_k, indicating an even stronger violation of the FL behavior when the hot spot coincides with a saddle point of the electronic spectrum.

For $M > 0$ and $\xi_k \ll M$ we take $x = r\cos\theta$, $y = r\sin\theta$ and $z = (\frac{\cos\theta^2}{2m_x} - \frac{\sin\theta^2}{2m_y})r^2 \equiv A_\theta r^2$, where $A_\theta \simeq \eta(\theta_0 - \theta)$, $\theta_0 = \arctan\sqrt{m_y/m_x}$ and η is a suitable constant, so that (12) becomes

$$\frac{1}{\tau_k} \simeq 4\lambda\nu t a^2 \int_0^{\theta_0} \frac{d\theta}{A_\theta} \int_0^1 dz \frac{1 - z}{(1 - z)^2 + \left(\frac{\nu a^2}{4A_\theta} z + \frac{M}{\xi_k}\right)^2} \sim \frac{\lambda a^2 t \nu}{2\eta} \left(\frac{\xi_k}{M}\right)^2 \log\left(\frac{M}{\xi_k}\right). \qquad (13)$$

and the van Hove singularity introduces a logarithmic correction to the FL behavior. In Fig. 1(b) we take $\mu/t = \bar{\mu}/t = -1.0$ and plot $1/\lambda\nu\tau_k$ as a function of ξ_k/ξ_{max}, according to (8), for k approaching $k_{HS} = (\pi/a, 0)$.

As M/t is reduced (by a factor of ten for each curve from bottom to top), the anomalous ξ_k-independent behavior extends over a wider range of energies. In particular, within the energy range considered in Fig. 1(b), the bottom curve ($M/t = 10^{-1}$) displays a FL behavior

(13), whereas the top curve ($M/t = 10^{-6}$) displays a non-FL ξ_k-independent behavior. The intermediate curves show the crossover from one regime to the other.

The enhancement of the phase-space available for scattering makes quasi-particles ill-defined in the vicinity of the hot spot. Moreover, as we shall show in the following, quasi-critical scattering near the hot spots does not only broaden the quasi-particle peak, but also suppresses of the polar behavior of the electron Green function near the Fermi energy.

In the model considered in this paper, where quasi-critical charge and spin fluctuations are simultaneously present, the hot spots corresponding to the different modes co-exist, leading to an extension of the anomalous behavior observed along the FS. This fact makes less stringent the objection in Ref. [26] about the limited effect of isolated hot spots on the behavior of the normal phase.

IV. QUASI-PARTICLE SPECTRA

In this section we discuss the properties of the self-energy (6,7) at $T = 0$. For the sake of clarity, we focus again on a single quasi-critical mode, dropping the index j. It must, however, be borne in mind that, once the relevant features are individuated, the physics of the system with coexisting charge and spin fluctuations results essentially (though not exactly) from a superposition of the separate effects.

The imaginary part (6), at a fixed k, is characterized by different features depending on the value of the energy ε compared to characteristic energy scales which we discuss in the following. For the sake of the discussion, in Fig. 2, we fix the parameters as $t = 200$ meV, $t' = -50$ meV and $\mu = -180$ meV (corresponding to a hole doping $x = 0.17$) for the electronic spectrum, $M = 2 \times 10^{-4}$ meV, $\nu = 1000$ meV and $Q = (\pi/a, \pi/a)$ for the fluctuation spectrum and we take a dimensionless coupling constant $\lambda = 0.2$. We also fix the external momentum $k = (1.32/a, 1.32/a)$, so that $\xi_k \simeq -10$ meV and $\xi_{k-Q} \simeq 390$ meV.

At energies $\varepsilon > \xi_{max}$ or $\varepsilon < \xi_{min}$ the integral in (6) extended over a domain which is independent of ε, so that $\mathrm{Im}\Sigma \simeq -C/\varepsilon$ as soon as $|\varepsilon| \gg \max(\xi_{max}, -\xi_{min}, 2\nu)$, where

$C = \frac{1}{2}\lambda t\nu[1 + x\ \mathrm{sgn}(\varepsilon)]$, x being the hole doping per unit cell. Broad dispersionless maxima for $|\mathrm{Im}\Sigma|$ are found at energies $\varepsilon \sim \min(\xi_{min}, -2\nu)$ and $\varepsilon \sim \max(\xi_{max}, 2\nu)$. Since in the case of Fig. 2(a) $2\nu > \xi_{max}, -\xi_{min}$, the maxima are found at energies $\varepsilon \simeq \pm 2\nu = \pm 2000$ meV.

Within the relevant range $\xi_{min} \leq \varepsilon \leq \xi_{max}$, two characteristic energy scales exist, M and ξ_{k-Q}. The first controls the low-energy behavior of $\mathrm{Im}\Sigma(k, \varepsilon \to 0)$, which may be obtained by generalizing the methods discussed in the previous section, to the case when ε varies independently of k. A FL behavior ($\sim \varepsilon^2$) is found for $|\varepsilon| \ll M^* \equiv M + \nu a^2 (\xi_{k-Q}/v_{k-Q})^2/2$ and a non-FL behavior ($\sim \sqrt{|\varepsilon|}$) is found for $M^* = 0$ (i.e. $M = 0$ and $\xi_{k-Q} = 0$). The case shown in Fig. 2 a corresponds to a low-energy FL behavior .

A particular role is played by the energy $\varepsilon = \xi_{k-Q}$, since both terms in the denominator of (6) vanish at $k' = k - Q$ (when $M = 0$). A peak, or a shoulder partially merged in the broad background structure discussed above is present in $\mathrm{Im}\Sigma$, depending on the parameters of the model. In Fig. 2(a) this point is marked by a diamond at an energy $\varepsilon \simeq 400$ meV. This dispersing structure *follows* the shadow band ξ_{k-Q} with varying k. As $\xi_{k-Q} \to 0$ the peak at $\varepsilon = \xi_{k-Q}$ is suppressed, due to the fact that $\mathrm{Im}\Sigma$ must vanish at the Fermi energy, but when $M = 0$ the usual FL behavior is turned into an anomalous square-root behavior which is present all along the curve $\xi_{k-Q} = 0$, usually called shadow FS. However it must be pointed out that such an anomalous behavior shows up in the quasi-particle properties only when the quasi-particle peak crosses the Fermi energy at the shadow FS, i.e. in the vicinity of the hot spots, where $\xi_k \simeq \xi_{k-Q} = 0$. Away from the hot spot, spectral weight is transferred from the quasi-particle peak to the shadow peak, leading to an enhancement of low-laying spectral weight along the shadow FS.

The real part of the self-energy, including a correction $\delta\mu \simeq -100$ meV to the chemical potential, found by solving Eq. (5) for the present set of parameters, is shown in Fig. 2 b. The presence of a peak in $\mathrm{Im}\Sigma$ at an energy $\varepsilon = \xi_{k-Q}$ produces a corresponding feature in $\mathrm{Re}\Sigma$ [marked by a diamond at $\varepsilon \simeq 400$ meV in Fig. 2(b)] which, unlike the case of Ref. [15], is not symmetric around $\varepsilon = \xi_{k-Q}$, due to the vanishing of (6) at $\varepsilon = 0$. As it will become clearer in the discussion of the quasi-particle spectra at the end of this section, the resulting

suppression of the quasi-polar structure of ReΣ turns the shadow-bands found in Ref. [15] into incoherent resonances at energies $\varepsilon \simeq \xi_{k-Q}$. We also point out that, in correspondence of the low-energy anomalous behavior $\sim \sqrt{|\varepsilon|}$, the suppression of the shadow feature in ReΣ is weaker than for the corresponding FL behavior ($\sim \varepsilon^2$).

In the regime of FL violation, at low energies Im$\Sigma = -A\mathrm{sgn}(\varepsilon)\sqrt{|\varepsilon|}$ and, by KKT, Re$\Sigma = -A\mathrm{sgn}(\varepsilon)\sqrt{|\varepsilon|}+B$, where A, B are constants, which depend on the parameters of the model. The electron Green function looses then its polar structure. If one however insists in assigning a polar structure to the Green function, the wave-function renormalization factor $Z = \{1 - [\mathrm{Re}\Sigma(\varepsilon) - \mathrm{Re}\Sigma(0)]/\varepsilon\}^{-1} \simeq A^{-1}\sqrt{|\varepsilon|}$ vanishes at the Fermi energy. The quasi-particle lifetime at the hot spots, $1/\tau_{qp} = 2Z|\mathrm{Im}\Sigma| = 2|\xi_k|$, turns out to be independent of the constants A, B. This behavior is a signature of the importance of considering the appropriate renormalizations when studying the transport properties in the presence of singular scattering. Thus this problem turns out to be more involved than usually considered [26].

The single-particle spectral properties are analyzed by means of the spectral density (4). The quasi-particle peak is located, for a given k, at the intercept between the straight line $y = \varepsilon - \xi_k$ and the curve $y = \mathrm{Re}\Sigma(k, \varepsilon)$. This intersection, in the weak-coupling limit $\lambda \ll 1$, is located at an energy close to ξ_k [$\varepsilon \simeq -40$ meV in Fig. 2(b)]. There is, however, a transfer of spectral weight to an energy $\varepsilon \simeq \xi_{k-Q}$, where the denominator in (4) has a local minimum [this point is marked by a diamond in Fig. 2(b)]. This incoherent spectral weight follows the dispersion of ξ_{k-Q} (or of all the ξ_{k-Q_j} in the general case when more fluctuating modes are present) giving rise to dispersing shadow resonances, which substitute in our approach the shadow bands found in Refs. [6,15]. As an example, in Fig. 3 spectra are shown along the ΓX direction in k space, away from the hot spots, for the same set of parameters as Fig. 2 and momenta $k_\ell = (\ell\pi/50a, \ell\pi/50a)$, with $\ell = 15, 17, 19, 21$. In this region of the Brillouin zone both the quasi-particle peak and the shadow peak have comparable intensities. As ξ_{k-Q} and ξ_k get closer to each other, an increasing amount of spectral weight is transferred from the quasi-particle peak to the shadow peak.

V. SPECTRAL DENSITY AND FERMI SURFACE IN ARPES EXPERIMENTS.

In this section we use the general results obtained above to discuss recent ARPES experiments Bi2212 near optimal doping [20,21,24,27,28]. The increasing experimental evidence for a stripe phase [12,13], reinforces our idea of having a charge modulation which enslaves a spin modulation, leading to the model (1) with coexisting charge and spin fluctuations. Thus, we deal here with the full self-energy (3) associated with critical modes of both types. We point out again that, when more than one mode is considered, the resulting effects are essentially a superposition of those discussed in the previous sections for a single generic mode. The presence of AFM fluctuations triggered by the incipient stripe instability is described, within our model, by the condition that both modes are quasi-critical, i.e. $M_c \leq M_s \ll t$. We neglect in the following the possibility for a modulation of the AFM characteristic wave-vector induced by stripe formation and the related splitting [10], which adds minor changes to the quantities under discussion, and does not appear to be resolved by ARPES data.

We make a comparison between the spectral density (4) and the experimental energy distribution curves (EDCs) [29] and we analyze the shape and properties of the FS. To reproduce typical conditions in ARPES experiments we introduce a convoluted spectral density

$$\tilde{A}_R(k,\varepsilon) = \int_{-\infty}^{+\infty} d\varepsilon' A(k,\varepsilon') f(\varepsilon') \mathcal{E}_R(\varepsilon' - \varepsilon) \tag{14}$$

which takes care of the absence of occupied states above the Fermi energy, through the Fermi function, and of the experimental energy resolution R, through the resolution function $\mathcal{E}_R(\varepsilon) = \exp(-\varepsilon^2/2R^2)/\sqrt{2\pi R^2}$. As it is customarily in ARPES experiments, the resolution in momentum space is assumed to be finer than the energy resolution, so that no convolution over k is performed in (14). A comparison is then possible between the experimental EDCs and the convoluted density (14) as a function of ε at given k. The self-energy which enters the expression (4) is evaluated here with a smooth cut-off $\Delta = 0.4$, which selects transferred momenta close to the characteristic wave-vectors Q_c, Q_s, to improve the agreement with experimental results [see Eq. (6) and the subsequent discussion].

A particular care is required to discuss the experimentally determined FS. Indeed, the presence of the shadow peaks and of the associated incoherent spectral weight at low energies along the shadow FS, makes the quasi-particle FS [determined by the equation $\xi_k + \mathrm{Re}\Sigma(k, \varepsilon = 0) = 0$] not appropriate. The ARPES EDCs reveal the FS via the zero-energy crossing of the dispersing intensity peaks, regardless of their coherence. More recently the FS was accurately determined as the distribution of spectral weight within an energy window around the Fermi energy, by means of the angle scanning photoemission (ASP) [20]. Once again the experimental distinction between the main and the shadow FS is lost. Thus, we associate with each k point the integrated spectral weight of low-laying occupied states

$$p_k^W = \int_{-W}^{W} A(k, \varepsilon) f(\varepsilon) d\varepsilon, \tag{15}$$

where $W \ll t$ [30], and we compare the distribution of p_k^W with the FS observed in ASP experiments [31]. We point out that, in the absence of an anomalous transfer of spectral weight to low energies, such a determination of the FS coincides essentially with the theoretical definition in terms of quasi-particle, at least for reasonably small W.

We want to discuss the evolution of the band structure as determined by following the intensity peaks in ARPES experiments and the properties of the FS, which is determined with more details in ASP experiments. To reproduce the experimental conditions in ARPES experiments [21] we take $T = 10$ meV and $R = 15$ meV in (14). To reproduce the conditions in ASP experiments [20] we take $T = 25$ meV and $W = 25$ meV in (15).

The parameters of the free-electron band ξ_k will be fixed to reproduce the band structure, the FS and the electron filling of Bi2212 at optimal doping, i.e. $t = 200$, $t' = -50$ meV, $\mu = -180$ meV, corresponding to a hole doping $x = 0.17$.

The experimentally observed FS in Bi2212 is approximately mirror-symmetric with respect to the $\Gamma X(Y)$ axes, but not with respect to the $\Gamma M(M_1)$ axes [20]. An additional feature of the experiments is the presence of a dispersing band along the ΓM direction, crossing the Fermi energy at $\tilde{k}_F = (0, 0.2\pi/a)$, which is absent along the ΓM_1 direction [28].

Within the stripe-QCP scenario, the symmetry of the FS is expected to be lowered by the

interaction between electrons and charge fluctuations, characterized by an incommensurate wave-vector Q_c, whereas in the presence of spin fluctuations only, the excitation spectrum and the FS are expected to have the full symmetry of the lattice, due to the peculiar commensurability of the characteristic wave-vector of the Néel AFM structure, $Q_s = (\pi/a, \pi/a)$. Within our model, in order to preserve the symmetry $k \to -k$, we always perform an average over $\pm Q_c$, i.e. we take a self-energy $\bar{\Sigma}_c = \frac{1}{2}[\Sigma_c(Q_c) + \Sigma_c(-Q_c)]$. Other point symmetries of the original system may be broken according to the direction of Q_c, which is system [10,32] and model dependent [33].

Based on the symmetry of the FS observed in Bi2212 [20], for this specific system we take $Q_c \simeq (0.4\pi/a, -0.4\pi/a)$, directed along the ΓY direction.

We discuss in some detail the case $\nu_c = \nu_s = 200$ meV, $M_c = M_s = 10$ meV and $\lambda_c = 1/2$, $\lambda_s = 1/6$ (to which Fig. 4 refers). The correction $\delta\mu$ to the chemical potential, obtained by solving Eq. (5) for the present set of parameters, is $\delta\mu = -40$ meV.

The single-particle spectra are characterized by the presence of shadow peaks associated with $\pm Q_c$ and Q_s. The two shadow peaks, associated with $\xi_{k\pm Q_c}$, and the corresponding branches of the shadow FS ($\xi_{k\pm Q_c} = 0$) do not coincide, as it is instead the case for the highly commensurate vector Q_s (which is equivalent to $-Q_s$).

In Fig. 4 the EDCs along the ΓM direction are reported in the panel on the right. The momentum k is increased from top to bottom by a uniform step $\Delta k = \pi/8a$. The quasi-particle peak moves from the left to the right towards the Fermi energy and interferes with the shadow peak associated with $+Q_c$ (see the third curve from the top) which moves initially to lower energies (fourth curve) and then again towards the Fermi energy. This shadow peak appears in Fig. 4 as a shoulder merged in the quasi-particle peak in the seventh curve from the top.

The shadow peak associated with Q_s is located at high energies above the Fermi level, near the Γ point. However, as k is increased, this peak moves towards the Fermi energy, while the quasi-particle looses spectral weight, which is transferred to the shadow peaks. In the last three curves in Fig. 4 the shadow peak associated with Q_s appears as a broad incoherent

peak moving towards an energy $\varepsilon \simeq -150$ meV while approaching the M point. We associate this peak with a corresponding feature observed in Bi2212 at an energy $\varepsilon \simeq -200$ meV [21].

For a comparison we report, in Figs. 5 and 6 respectively, the effects due to spin and charge modes when considered separately. In the right panel of Fig. 5, from top to bottom, the quasi-particle peak looses its weight as it moves towards the Fermi energy, while near the M point a broader shadow structure still appears below the Fermi energy. Recently this feature was discussed within the NAFL scenario in Ref. [25], where a full re-summation of the diagrammatic expansion in the static limit was performed. We point out, however, that these results match those obtained within our simpler perturbative approach. In the right panel of Fig. 6 we report the single-particle spectra in the ΓM direction in the presence of charge fluctuations only. The first six curves from the top are very similar to the corresponding curves in Fig. 4, since there the spin-related shadow peak is located at much higher energy above the Fermi level. The shadow peak related to $+Q_c$ appears to cross the Fermi level at $\tilde{k}_F \simeq (2.4/a, 0)$ in Fig. 6. In the last three curves, due to the absence of the effects related to spin fluctuations, the quasi-particle peak never reaches the Fermi energy along the γM direction. The van Hove singularity is located at $\xi_{VH} \simeq -50$ meV.

The description of the additional feature observed only in the ΓM direction [28] would require the introduction of an additional charge modulation wit a wave-vector $Q_c' \simeq (0, 2\pi/3a)$. We do not discuss these finer details here.

We now discuss the properties of the FS according to the distribution (15) of low-laying spectral weigh. The main features of the FS, reported in the left panel of Fig. 4, are an inhomogeneous distribution of spectral weight, which is maximum near the diagonals of the Brillouin zone, and an asymmetric suppression of spectral weight near the $M(M_1)$ points, as experimentally observed [20]. The first aspect is related to the evolution of the FS in the underdoped regime, as the temperature is lowered down to the superconducting critical temperature [34]. We point out that, since we are at a fixed doping $x = 0.17$, and since our model (1) is inadequate to discuss the underdoped regime, where the spectrum of charge fluctuations is presumably modified by the presence of preformed Cooper pairs, we can only

describe the onset of this evolution. The second aspect is understood as a co-operative effect of spin fluctuations, which lead to a symmetric suppression (see the left panel in Fig. 5, where spin fluctuations only are considered), and charge fluctuations, which introduce an asymmetric modulation related to the direction and magnitude of Q_c (see the left panel in Fig. 6, where charge fluctuations only are considered).

The branches of the shadow FS due to charge fluctuations, which are clearly visible in Fig. 6, where they cross transversally the $\Gamma M(M_1)$ directions in the vicinity of the $M(M_1)$ points, interfere with the branches due to spin fluctuations, when both mode are considered as in Fig. 4.

Another feature of the FS, related to spin fluctuations, is the possibility for the presence of hole pockets around the points $(\pm\pi/2a, \pm\pi/2a)$ of the Brillouin zone. According to our interpretation of the experimentally observed FS we choose a set of parameters which leads to very weak hole pockets, which are well below the threshold fixed for the representative points in Figs. 4 and 5, and are not reported. Larger $|t'/t|$, and/or larger ν_s/t, and/or a sharper cut-off Δ, and/or a smaller energy window W, make this phenomenon more pronounced¿ Whenever present, the hole pockets are not associated with a topological change of the quasi-particle FS, as in Ref. [6], but rather correspond to a distribution p_k^W which is characterized by local maxima at the FS ($\xi_k = 0$) and at the branch of the shadow FS ($\xi_{k-Q_s} = 0$), and minima at $(\pm\pi/2a, \pm\pi/2a)$. The experimental situation is still controversial within this respect. Shadow bands shifted by a wave-vector Q_s and/or the related hole pockets were reported in Refs. [20,24,35] but were not detected in Refs. [21,34].

VI. CONCLUSIONS

We studied the changes in the single-particle properties due to the coupling of electrons to quasi-critical charge and spin fluctuations in the quantum critical region around a stripe QCP. Violations to the normal FL behavior appear in the on-shell inverse scattering time, at those points of the FS connected by a characteristic wave-vector of the critical fluctuations

(hot spots). The violations are stronger when a hot spot is located near a singular point of the electronic spectrum, leading to a finite inverse scattering time. This result may be relevant for the physics of high-T_c cuprates, where extended van Hove singularities have been repeatedly observed [36] close to the Fermi energy at the M points, in the presence of critical fluctuations characterized by either a large ($\sim Q_s$) or a small Q_c wave-vector, leading to hot spots in the vicinity of the M points.

The study of the quasi-particle spectra showed that the violation to the FL behavior are associated with the transfer of spectral weight from the quasi-particle band to incoherent shadow peaks. These feature are dispersing and show up in the ARPES EDCs, though they do not correspond to poles of the electron Green function. As the shadow peaks approach the Fermi level, they produce an enhancement of low-laying spectral weight which is seen as a shadow FS within a finite energy resolution.

The evolution of the FS is thus associated with the change in the distribution of the low-laying spectral weight and not with the topological modification of the quasi-particle FS proposed in Ref. [6].

The quasi-particle spectra and the FS obtained within the model with coexisting charge and spin fluctuations capture the relevant features observed in ARPES experiments on optimally doped Bi2212, and namely the presence of broad features in the EDCs (besides the quasi-particle peak) the inhomogeneous distribution of spectral weigh along the FS and the asymmetric suppression of spectral weight around the $M(M_1)$ points of the Brillouin zone [37].

On the other hand we suggest that the ARPES experiments may be used to extract informations about the parameters entering in the fluctuation spectra (2), which can then be tested consistently within the theory. In particular, the direction and magnitude of Q_c might be deduced from the modulation in the suppression of spectral weight along branches of the FS, as suggested in Ref. [20], or from a systematic, and still lacking, investigation of the related shadow peaks.

Acknowledgements: Part of this work was carried out with the financial support of

the INFM, PRA 1996. The authors would like to thank Prof. C. Castellani for many useful discussions and suggestions.

REFERENCES

[1] S. Sachdev and J. Ye, *Phys. Rev. Lett.* **69**, 2411 (1992).

[2] P. Monthoux and D. Pines, *Phys. Rev.* **B 50**, 16015 (1994).

[3] P. Monthoux, A. V. Balatsky and D. Pines, *Phys. Rev.* **B 46**, 14803 (1992); A. Sokol and D. Pines, *Phys. Rev. Lett.* **71**, 2813 (1993).

[4] C. Castellani, C. Di Castro and M. Grilli, *Phys. Rev. Lett.* **75**, 4650 (1995).

[5] J. Rossat-Mignod, *et al.*, Physica Scripta **T 45**, 74 (1992); T. E. Mason, *et al.*, Physica **B 199-200**, 284 (1994); T. E. Mason, *et al.*, *Phys. Rev. Lett.* **77**, 1604 (1996); P. Bourges, *et al.*, *Phys. Rev.* **B 53**, 876 (1996); S. Petit, *et al.*, *Physica* **B 234-236**, 800 (1997); G. Aeppli, *et al.*, *Science* **278**, 1432 (1997) and references therein; T. Suzuki, *et al.*, *Phys. Rev.* **B 57**, R3229 (1998); Pengcheng Dai, H. A. Mook and F. Doğan, *Phys. Rev. Lett.* **80**, 1738 (1998).

[6] A. V. Chubukov, D. K. Morr and A. Shakhnovich, Phil. Mag. **B 74**, 563 (1996). A. V. Chubukov and D. K. Morr, *Phys. Rep.* **288**, 347 (1998).

[7] V. J. Emery, S. A. Kievelson and H. Q. Lin, *Phys. Rev. Lett.* **64**, 475 (1990); M. Marder, N. Papanicolau and G. C. Psaltakis, *Phys. Rev.*, **41**, 6920 (1990); M. Grilli, *et al.*, *Phys. Rev. Lett.* **67**, 259 (1991); N. Cancrini, *et al.*, *Europhys. Lett.* **14**, 597 (1991); R. Raimondi, *et al.*, *Phys. Rev.* **B 47**, 3331 (1993); S. Caprara, C. Di Castro and M. Grilli, *Phys. Rev.* **B 51**, 9286 (1995); F. Bucci, *et al.*, *Phys. Rev.* **B 52**, 6880 (1995); M. Grilli and C. Castellani, *Phys. Rev.* **B 50**, 16880 (1994).

[8] F. Becca, *et al.*, *Phys. Rev.* **B 56**, 12443 (1996).

[9] G. S. Boebinger, *et al.*, *Phys. Rev. Lett.* **77**, 5417 (1996).

[10] J. M. Tranquada, *et al.*, *Nature* **375**, 561 (1995); J. M. Tranquada, *et al.*, *Phys. Rev.* **B 56**, 7689 (1996).

[11] A. Bianconi, *et al.*, *Phys. Rev. Lett.* **76**, 3412 (1996).

[12] A. Bianconi, *et al.*, *Phys. Rev.* **54**, 12018 (1996).

[13] A. Bianconi, *et al.*, *Phys. Rev.* **B 54**, 4310 (1996).

[14] A. Bianconi, *Physica* **C 235-240**, 269 (1994).

[15] A. P. Kampf and J. R. Schrieffer, *Phys. Rev.* **B 42**, 7967 (1990).

[16] A. Bombardi, A. Di Stasio, and A. Tagliacozzo, unpublished.

[17] We point out that the theory proposed in Ref. [15] is based on a modification of the mean-field susceptibility, and not of the mean-field self-energy. However this difference is unessential as far as a qualitative discussion of the properties of the resulting quasi-particle spectra is concerned.

[18] A. J. Millis, H. Monien and D. Pines, *Phys. Rev.* **B 42**, 167 (1990).

[19] See, e.g., the proceedings of the Second International Conference *Stripes and High-T_c Superconductivity*, Rome 2-6 June 1998, to appear in J. of Supercond., (1999).

[20] N. L. Saini, *et al.*, *Phys. Rev. Lett.* **79**, 3464 (1997).

[21] D. S. Marshall, *et al.*, *Phys. Rev. Lett.* **76**, 4841 (1996).

[22] M. Langer, J. Schmalian, S. Grabowski and K. H. Bennemann, *Phys. Rev. Lett.* **75**, 4508 (1995); M. Langer, J. Schmalian, S. Grabowski and K. H. Bennemann, *Phys. Letters A* **212**, 270 (1996); S. Grabowski, J. Schmalian, M. Langer and K. H. Bennemann, *Solid State Commun.* **98**, 611 (1996); M. Langer, J. Schmalian, S. Grabowski and K. H. Bennemann, *Solid State Commun.* **97**, 663 (1996).

[23] For a different interpretation of the broad features appearing in ARPES data see, e.g., S.-X. Shen and J. R. Schrieffer, *Phys. Rev. Lett.* **78**, 1771 (1997).

[24] S. La Rosa, *et al.*, *Solid State Commun.* **104**, 459 (1997).

[25] J. Schmalian, D. Pines and B. Stojković, *Phys. Rev. Lett.* **80**, 43839 (1998).

[26] R. Hlubina and T. M. Rice, *Phys. Rev.* **B 51**, 9253 (1995).

[27] J. M. Harris, *et al.*, *Phys. Rev. Lett.* **79**, 143 (1997).

[28] N. L. Saini, *et al.*, *Phys. Rev.* **B 57**, R11101 (1998).

[29] The need for an accurate analysis of the experimental EDCs in terms of a spectral function including many-body effects was recently re-stated by N. L. Saini, *et al.*, proceedings of the Second International Conference *Stripes and High-T_c Superconductivity*, Rome 2-6 June 1998, to appear in J. of Supercond., (1999).

[30] We assume here a different meaning for the experimental resolution in ARPES and ASP experiment. It is, however, evident that $p_k^W \simeq \sqrt{2\pi W^2}\tilde{A}_{R=W}(k, \varepsilon = 0)$.

[31] In more detail, such weights are grouped into classes according to the value of the class index $i = [1 - \log_b(p_k^W/p_{max}^W)]$, where the square brackets select the integer part, b is a suitably chosen basis and p_{max}^W is the maximum over k of p_k^W. Each value of $i = 1, 2, ...$ corresponds to a weight $p_{max}^W/b^i < p_k^W \leq p_{max}^W/b^{i-1}$. We plot points with $i \leq i_0$, where i_0 represents the threshold of the experimental apparatus.

[32] H. A. Mook, proceedings of the Second International Conference *Stripes and High-T_c Superconductivity*, Rome 2-6 June 1998, to appear in J. of Supercond., (1999).

[33] G. Seibold, *et al.*, cond-mat/9803184 to appear in Phys. Rev. **B**, (1998).

[34] M. R. Norman, *et al.*, *Nature* **392**, 157 (1998).

[35] P. Aebi, *et al. Phys. Rev. Lett.* **72**, 2757 (1994).

[36] D. S. Dessau, *et al.*, *Phys. Rev. Lett.* **71**, 2781 (1993); D. M. King, *et al.*, *Phys. Rev. Lett.* **73**, 3298 (1994); K. Gofron, *et al.*, *Phys. Rev. Lett.* **73**, 3302 (1994); J. Ma, *et al.*, *Phys. Rev.* **B 51**, 3832 (1995); J. C. Campuzano, *et al.*, *Phys. Rev.* **B 53**, R14737 (1996).

[37] We are aware of the fact that the intrinsic modulation of the Bi-planes in the $(1,-1)$ direction introduces satellites branches of the FS [38] due to the umklapp of photo-electrons which are scattered by the periodic Bi-planes before reaching the detector. However such an effect seems not to be sufficient to explain the asymmetric distribution of spectral weight around the $M(M_1)$ points, since the weight of the satellites branches is too small to produce the observed intensities.

[38] H. Ding, *et al.*, *Phys. Rev. Lett.* **76**, 1533 (1996).

FIGURE CAPTIONS

Fig. 1: Dimensionless on-shell inverse scattering time at the hot spot, as a function of ξ_k/ξ_{max}. (a) The parameters of the electronic spectrum are $t'/t = -0.25$, $\mu/t = -0.9$ (corresponding to a hole doping $x = 0.17$); the parameters of the fluctuation spectrum are $\nu/t = 5.0$, $Q = (\pi/a, \pi/a)$, while M/t varies in the range $[10^{-6}; 10^{-1}]$ increasing by a factor of 10 for each curve from top to bottom. The hot spot is located at $k_{HS} = (0.32/a, 2.82/a)$. (b) Same parameters as in (a), except for the chemical potential $\mu/t = -1.0$ (corresponding to a hole doping $x = 0.22$). The van Hove singularity in the electronic spectrum is located at the Fermi level. The hot spot is located at $k_{HS} = (\pi/a, 0)$.

Fig. 2: Self-energy as a function of the external energy ε. The parameters are the same as in Fig. 1(a), with $t = 200$ meV, to fix the energy scale, and $M/t = 10^{-6}$. The dimensionless coupling is $\lambda = 0.2$ and the momentum is $k = (1.32/a, 1.32/a)$. For these values of the parameters $\xi_k \simeq -10$ meV and $\xi_{k-Q} \simeq 390$ meV (marked by a diamond on the energy axis). (a) Imaginary part. The broad dispersionless maxima are located at $\varepsilon \simeq \pm 2000$ meV. The shadow feature is located at $\varepsilon = \xi_{k-Q}$. (b) Real part, including a correction to the chemical potential $\delta\mu \simeq -100$ meV. The shadow feature is located at $\varepsilon = \xi_{k-Q}$. The quasi-particle peak corresponds to the intercept between the solid line $\varepsilon - \xi_k$ and the curve $\mathrm{Re}\Sigma(k, \varepsilon)$, and is located at an energy $\varepsilon \simeq -50$ meV. The dashed lines represent the axes.

Fig. 3: Spectral density for $k_\ell = (\ell\pi/50a, \ell\pi/50a)$, with $\ell = 15, 17, 19, 21$ (dot-dashed, dotted, dashed and solid lines respectively). The other parameters are the same as in Fig. 2. The quasi-particle peak is moving from the left to the right (towards the Fermi energy) as ℓ is increased. The shadow peak is moving from the right to the left as ℓ is increased. The position of the shadow band, $\varepsilon = \xi_{k-Q}$, is marked by diamonds on the energy axis. Spectral weight is transferred from the quasi-particle peak (on the left) to the shadow peak (on the right) as the two peak get closer to each other.

Fig. 4: LEFT: Distribution of low-laying spectral weight p_k^W within the Brillouin zone in the case of electrons coupled to both charge and spin fluctuations. The weight is reduced by a factor of 2 as the size of the black squares is reduced. Four classes are shown. The

weight less than 1/16 of the maximum is not reported. The parameters of the electronic spectrum are $t = 200$ meV, $t' = 50$ meV, $\mu = -180$ meV (corresponding to a hole doping $x = 0.17$). The parameters of the fluctuation spectra are $\nu_{s,c} = 200$ meV, $M_{s,c} = 10$ meV, $Q_s = (\pi/a, \pi/a)$ and $Q_c = (0.4\pi/a, -0.4\pi/a)$. The dimensionless coupling constants are $\lambda_s = 1/6$, $\lambda_c = 1/2$ and the dimensionless cut-off is $\Delta = 0.4$. The correction to the chemical potential is $\delta\mu \simeq -40$ meV. The integrated spectral weight p_k^W is calculated according to (15) with $W = 25$ meV and $T = 25$ meV. RIGHT: Convoluted spectral density $\tilde{A}_R(k, \varepsilon)$, calculated according to (14) with $R = 10$ meV and $T = 10$ meV, along the ΓM direction for the same parameters as in the left panel. The momentum is uniformly increased from top to bottom.

Fig. 5: LEFT: Distribution of low-laying spectral weight p_k^W within the Brillouin zone in the case of electrons coupled to spin fluctuations only. The weight is reduced by a factor of 2 as the size of the black squares is reduced. Four classes are shown. The weight less than 1/16 of the maximum is not reported. The parameters of the electronic spectrum are the same as in Fig. 4. The parameters of the spin-fluctuation spectrum are $\nu_s = 200$ meV, $M_s = 10$ meV, $Q_s = (\pi/a, \pi/a)$. The dimensionless coupling constant is $\lambda_s = 1/3$ and the dimensionless cut-off is $\Delta = 0.4$. The correction to the chemical potential is $\delta\mu = -70$ meV. The integrated spectral weight p_k^W is calculated according to (15) with $W = 25$ meV and $T = 25$ meV. RIGHT: Convoluted spectral density $\tilde{A}_R(k, \varepsilon)$, calculated according to (14) with $R = 10$ meV and $T = 10$ meV, along the ΓM direction for the same parameters as in the left panel. The momentum is uniformly increased from top to bottom.

Fig. 6: LEFT: Distribution of low-laying spectral weight p_k^W within the Brillouin zone in the case of electrons coupled to charge fluctuations only. The weight is reduced by a factor of 2 as the size of the black squares is reduced. Four classes are shown. The weight less than 1/16 of the maximum is not reported. The parameters of the electronic spectrum are the same as in Fig. 4. The parameters of the charge-fluctuation spectrum are $\nu_c = 200$ meV, $M_c = 10$ meV, $Q_c = (0.4\pi/a, -0.4\pi/a)$. The dimensionless coupling constant is $\lambda_c = 1/2$ and the dimensionless cut-off is $\Delta = 0.4$. The correction to the chemical potential

is negligible. The integrated spectral weight p_k^W is calculated according to (15) with $W = 25$ meV and $T = 25$ meV. RIGHT: Convoluted spectral density $\tilde{A}_R(k, \varepsilon)$, calculated according to (14) with $R = 10$ meV and $T = 10$ meV, along the ΓM direction for the same parameters as in the left panel. The momentum is uniformly increased from top to bottom.

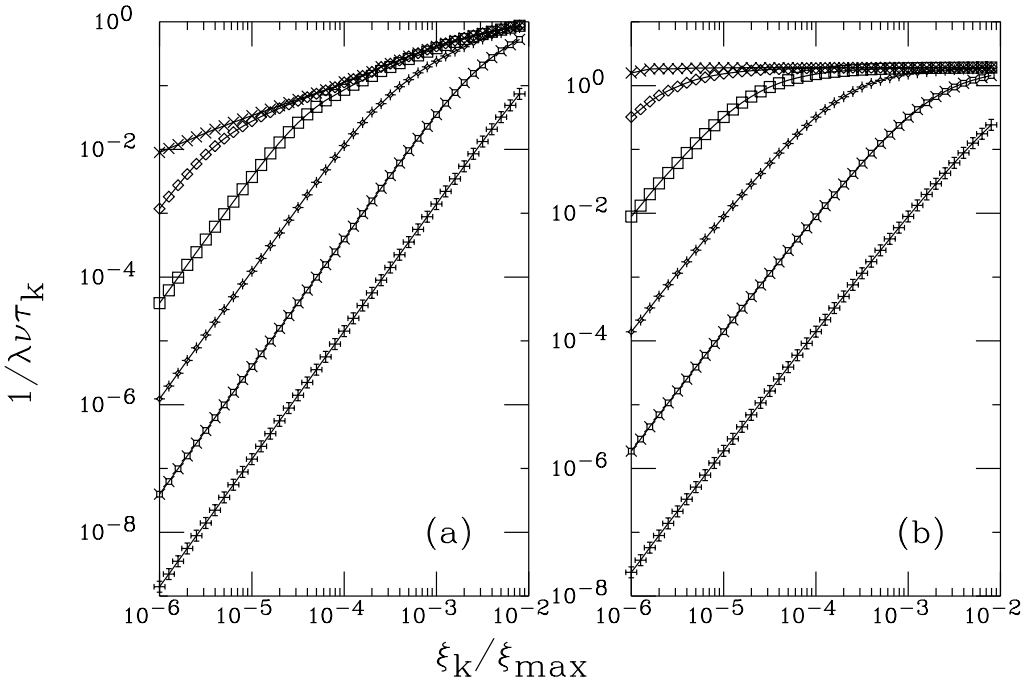

FIG. 1. S. Caprara *et al.* - *Single-particle properties of a model ...*

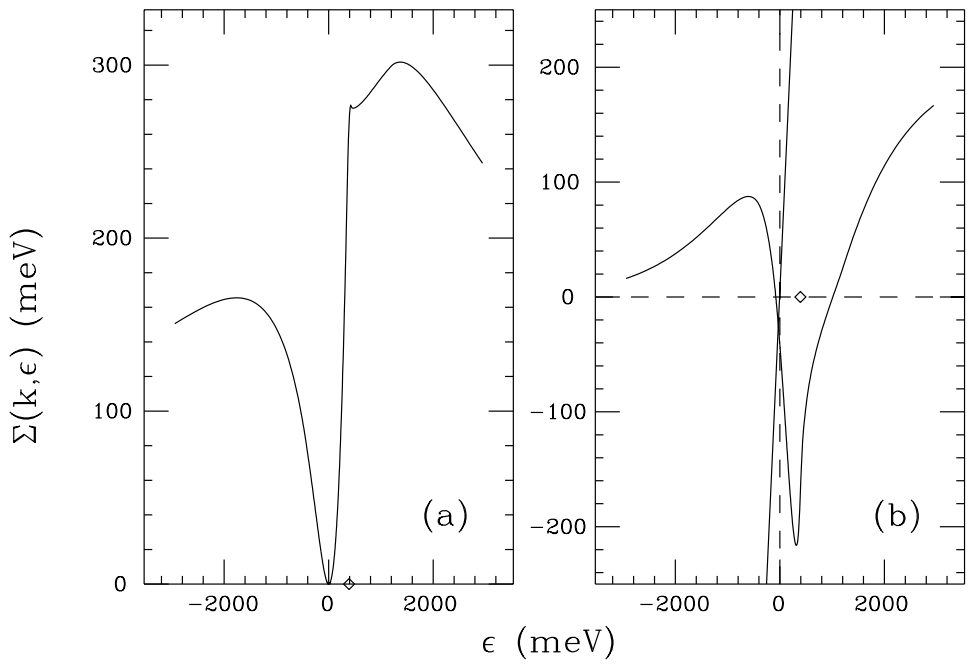

FIG. 2. S. Caprara *et al.* - *Single-particle properties of a model ...*

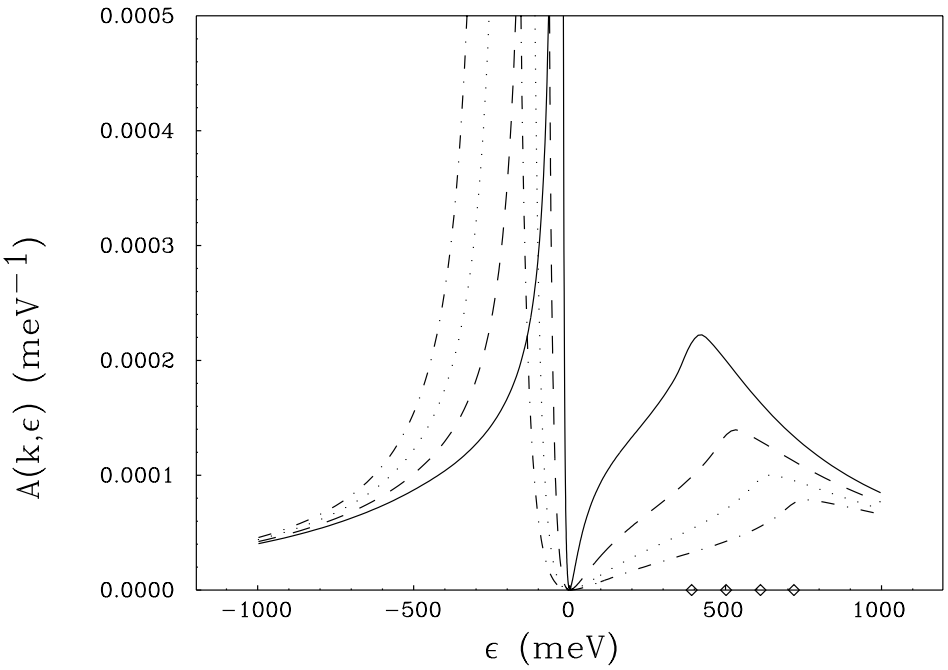

FIG. 3. S. Caprara *et al.* - *Single-particle properties of a model ...*

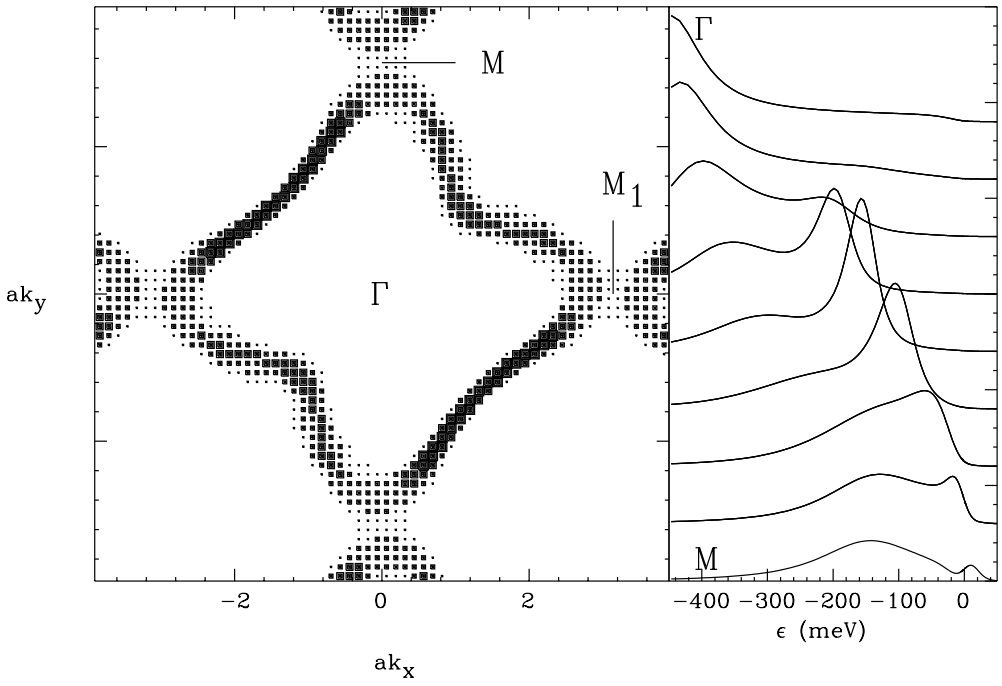

FIG. 4. S. Caprara *et al.* - *Single-particle properties of a model ...*

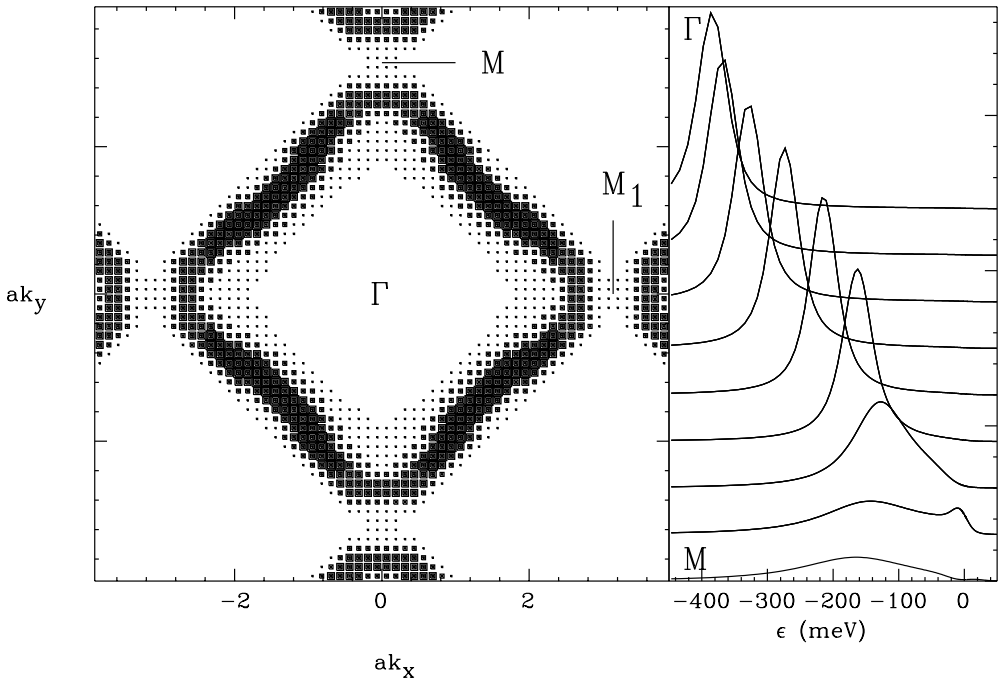

FIG. 5. S. Caprara *et al.* - *Single-particle properties of a model ...*

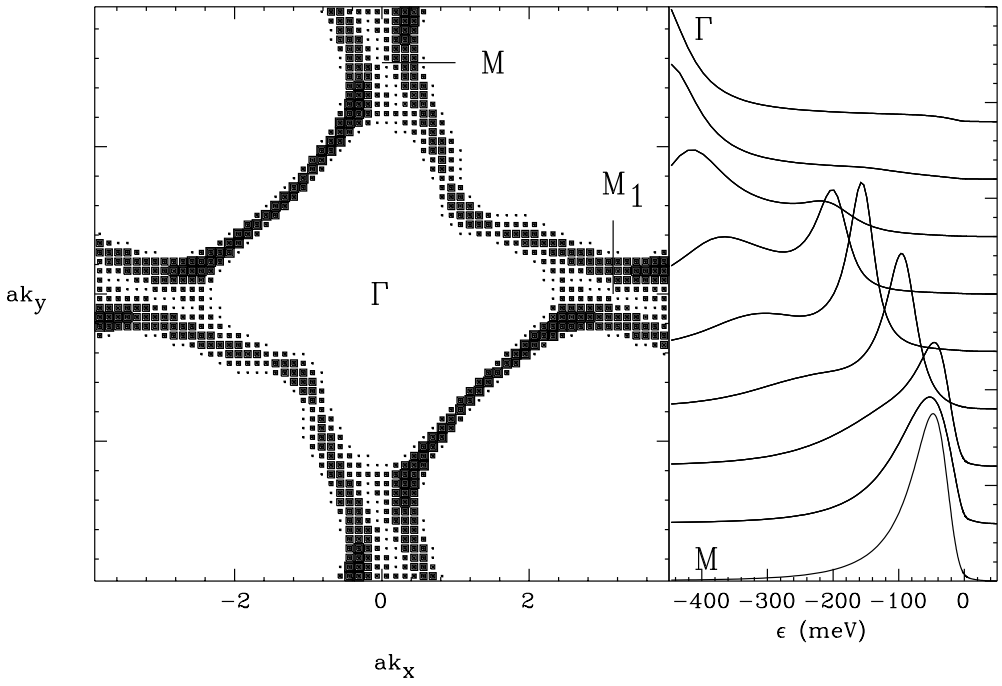

FIG. 6. S. Caprara *et al.* - *Single-particle properties of a model ...*